Journal of Neurotrauma

DOI: 10.1089/neu.2020.7225

Impaired glutamate receptor function underlies early activity loss of ipsilesional motor cortex following closed-head mild traumatic brain injury

Tyler Nguyen[1,2], Mohammed Haider Al-Juboori[3], Jakub Walerstein[1], Wenhui Xiong[1], Xiaoming Jin[1*]

[1]Indiana Spinal Cord and Brain Injury Research Group, Stark Neuroscience Research Institute & Department of Anatomy, Cell Biology and Physiology, Indiana University School of Medicine, Indianapolis, Indiana.

[2]Medical Neuroscience Program, Stark Neuroscience Research Institute, Indiana University School of Medicine, Indianapolis, Indiana.

[3]Indiana Spinal Cord and Brain Injury Research Group, Stark Neuroscience Research Institute & Department of Neurological Surgery, Indiana University School of Medicine, Indianapolis, Indiana.

Tyler Nguyen: ptnguyen@iu.edu 320 W. 15th Street, NB-500, Indianapolis, IN, USA 46202 (Tel: 502-295-8792)

Mohammed Haider Al-juboori: mohmalik@iu.edu 320 W. 15th Street, NB-500, Indianapolis, IN, USA 46202 (Tel: 317-278-5786)

Jakub Walerstein: jakub.d.w@gmail.com 320 W. 15th Street, NB-500, Indianapolis, IN, USA 46202 (Tel: 317-278-5786)

Wenhui Xiong: wxiong@iupui.edu 320 W. 15th Street, NB-500, Indianapolis, IN, USA 46202 (Tel: 317-278-5786)

Xiaoming Jin xijin@iupui.edu 320 W. 15th Street, NB-500, Indianapolis, IN, USA 46202 (Tel: 317-278-5786)

Nguyen, T., Al-Juboori, M. H., Walerstein, J., Xiong, W., & Jin, X. (2020). Impaired Glutamate Receptor Function Underlies Early Activity Loss of Ipsilesional Motor Cortex after Closed-Head Mild Traumatic Brain Injury. Journal of Neurotrauma. https://doi.org/10.1089/neu.2020.7225

* Corresponding author: Xiaoming Jin, PhD, Indiana Spinal Cord and Brain Injury Research Group, Stark Neuroscience Research Institute & Department of Anatomy, Cell Biology and Physiology, Indiana University School of Medicine, 320 West 15th Street, NB 500C, Indianapolis, IN 46202. Tel: (317) 278-5766; Fax: (317) 231-0203; Email: xijin@iupui.edu.

Abstract:

Although mild traumatic brain injury (mTBI) accounts for majority of TBI patients, the effects and cellular and molecular mechanisms of mild TBI on cortical neural circuits are still not well understood. Given the transient and non-specific functional deficits following mTBI, it is important to understand whether mTBI causes functional deficits of the brain and the underlying mechanism, particularly during the early stage after injury. Here we used in vivo optogenetic motor mapping to determine longitudinal changes in cortical motor map and in vitro calcium imaging to study how changes in cortical excitability and calcium signals may contribute to the motor deficits in a closed-head mTBI model. In Channelrhodopsin 2 (ChR2)-expressing transgenic mice, we recorded electromyograms (EMG) from biceps muscles induced by scanning blue laser on the motor cortex. There were significant decreases in the size and response amplitude of motor maps of the injured cortex at 2 hours post-mTBI but an increase in motor map size of the contralateral cortex in 12 hours post-mTBI, both of which recovered to baseline level in 24 hours. Calcium imaging of cortical slices prepared from GCaMP6-expressing transgenic mice showed a lower amplitude but longer duration of calcium transients of the injured cortex in 2 hours post-mTBI. Blockade of AMPA or NMDA receptors resulted in smaller amplitude of calcium transients, suggesting impaired function of both receptor types. Imaging of calcium transients evoked by glutamate uncaging revealed reduced response amplitudes and longer duration in 2, 12, and 24 hours after mTBI. Higher percentages of neurons of the injured cortex had longer latency period after uncaging than that of the uninjured neurons. The results suggest that impaired glutamate neurotransmission contributes to functional deficits of the motor cortex in vivo, which supports enhancing glutamate neurotransmission as a potential therapeutic approach for the treatment of mTBI.

Keywords: optogenetic mapping; calcium imaging; controlled cortical impact (CCI); Traumatic Brain Injury (TBI); neuroplasticity;

Introduction

Traumatic brain injury (TBI), as occurs in fallings, sports, and automobiles accidents, is a leading cause of death and disability among people aged 1 to 44 years[1]. Of all 1.7 million individuals who sustain a TBI annually, about 75% of them suffer concussion, a mild form of TBI (mTBI). In contrast to severe TBI that results in skull penetration, hemorrhage, and edema, mTBI patients present with a focal and diffuse injury resulting from non-penetrating head blow. The focal impact is produced by forces acting on the skull that results in local tissue compression beneath the impact site[2] , while diffuse impact is produced by a rapid acceleration-deceleration of the head that results in diffuse axonal injury, brain swelling, and hypoxic ischemic damage[3].

The effects of cellular and molecular perturbations following mTBI are still largely unknown and are sometimes conflicting among different studies. In severe TBI, in addition to impairments including edema, increased intracranial pressure and hemorrhages, release of excessive glutamate and activation of glutamate receptors are believed to cause intracellular calcium overload, neuronal death, and behavioral deficits[7, 8]. Consequently, blocking glutamate receptor activation has generated impetus within the brain trauma research community and pharmaceutical industry for the treatment of TBI. However, several studies indicate that an increase in synaptic glutamate release may be a transient event, lasting approximately 8-10 minutes after mTBI[9] and 30 minutes after severe TBI[10]. Furthermore, surface expressions of glutamatergic receptors including N-methyl-D-aspartate (NMDA) receptors and α-amino-3-hydroxy-5-methyl-4-isoxazolepropionic acid (AMPA) receptors have been shown to be reduced in many brain areas, especially in motor cortex, while activating NMDA receptors, rather than inhibiting them, can improve motor and cognitive behavior of TBI mice in long term [11, 12]. More recent studies demonstrated ineffectiveness or unreliable effectiveness of blocking glutamate receptors as a treatment for TBI in both animal models[14] and human clinical trials[15]. In particular, a phase III clinical study found that treating severe TBI patients with an NMDA receptor antagonist Selfotel actually resulted in worsening, rather than improving, of the symptoms[15]. Therefore, understanding the time course of cortical functional deficits after brain injury and further

examining the role of glutamate excitotoxicity is important to developing effective treatment strategy for mTBI.

Given the transient and non-specific functional deficits following mTBI, there is a lack of insight into the changes in brain function and the underlying mechanism, particularly during the early stage after injury. The recent optogenetic motor mapping technique provides a powerful tool for longitudinally studying dynamic changes of cortical circuits after mTBI [4-6]. Here for the first time in mTBI study, we used an in vivo optogenetic mapping technique to repeatedly map motor cortex of ChannelRhodopsin 2 (ChR2)-expressing transgenic mice to determine longitudinal changes in cortical motor map after closed-head mTBI. We then imaged calcium signals of spontaneous and glutamate-uncaging evoked activities in brain slices from GCaMP6 transgenic mice to determine whether dysfunctions of NMDA and AMPA receptors underlay such functional deficits. Our results suggest that reduced functions of these two ionotropic glutamate receptors contributed to the in vivo functional deficits observed after mTBI.

Materials and Methods

Animals: All animal procedures were approved by the Institutional Animal Care and Use Committee (IACUC) of the Indiana University School of Medicine. Wild type C57BL/6J (The Jackson Laboratory, Jax #000664) mice at 5-7 weeks old (~20-25 g) were divided into sham and injury groups. For slice imaging experiments, GCaMP6f (The Jackson Laboratory, Jax #024276) transgenic mice at 5-7 weeks old were divided into multiple groups for different time points after mTBI.

Preparation of mTBI model: mTBI was created using a technique described recently[16, 17]. Before injury, mice were anesthetized with a mixture of ketamine (87.7 mg/mL) and xylazine (12.3 mg/mL) and placed in a stereotaxic frame. A heating pad was placed underneath their abdomen to maintain body temperature. The scalp of a mouse was removed to expose the skull between the Bregma and Lamda positions. The periosteum of the skull was removed and cleaned thoroughly and dried with air flow for ~20 sec. A thin layer of cryano-acrylate glue was applied to cover the exposed skull. After the mouse head was stereotactically fixed, a closed-head mTBI was produced using a

control cortical impact (CCI) device with a modified impactor tip via attaching a 3-mm diameter round silicone tip of 1.5 mm thickness on it (Benchmark Stereotaxic Impactor, Leica Impactor One, Meyer Instrument, St. Louis, MO). After the baseline point of the device was set by lowering the tip to the skull surface and the stage position was set to zero, the impactor was retracted and the impact depth was set. The approximate center of the impact site was 1 mm posterior to the bregma and 0.5 mm lateral from midline on one cortical hemisphere. The skull was hit with the impactor tip at a speed of 4 m/s to a depth of 2 mm. All animals survived the injury without any skull fracture or hemorrhage.

In-vivo optogenetic mapping of motor cortex: Optogenetic mapping of bilateral motor cortex was made using a previous described technique [5]. Briefly, mice were anesthetized with a mixture of ketamine (83.85 mg/ml) and xylazine (8.15 mg/ml) and fixed in a stereotaxic frame. This modified mixture of ketamine and xylazine was used for in vivo motor mapping because it allowed us to keep the mice in a shallow anesthetic state but without completely blocking motor response as the usual concentrations of ketamine and xylazine do. The mice were maintained in an anesthetic level such that they were motionless but responsive to tail pinch throughout the course of experiment. An optogenetic mapping setup was used to control the scanning of a 470-nm laser (5 ms duration) on the skull. Each mapping region consisted of a rectangular grid of 5 x 6 spots with 300 µm spacing between adjacent spots (1.5-by-1.8 mm). Laser pulses were applied onto each spot at a random order until all spots were covered. Mapping area of each cortical hemisphere consisted of six mapping grids, with a total dimension of 4500 x 3600 µm. Evoked electromyogram (EMG) was recorded with an electrode inserted into anterior biceps brachii of the contralateral forelimb. The signals were amplified using a DP-304 Differential Amplifier (Warner Instrument Corp), digitized with a DigiData acquisition system (model 1550B, Molecular Devices), and recorded in pClamp 9 (Axon Instruments, Molecular Devices). For each animal, each cortical region was mapped repeatedly for three times and spots with two or three responses were counted as active spots. Spots with zero or one response was considered as unresponsive.

The EMG responses were detected and analyzed using Detector Analysis software[5]. The amplitude for each stimulated spot was averaged from the amplitudes of two or three

repetitions. The numbers of active spots were obtained by counting the spots that produced EMG responses. Average EMG amplitudes with respect to anterior-to-posterior and medial-to-lateral axis were calculated by averaging all response amplitudes for all active spots along the direction of interest. Motor cortical activity maps were constructed with OriginPro 9.1 (OriginLab, Northampton, MA).

Cortical slice preparation: GCamp6 mice were anesthetized with 78 mg/kg ketamine and 22 mg/kg xylazine (intraperitoneally) and decapitated with scissors. After the scalp was removed, the skull was cut along the mid-sagittal line and the two flaps of bone covering both brain hemispheres were removed. The brain was then taken out and immediately placed in an ice-cold 4 ^{o}C oxygenated sucrose artificial cerebral spinal fluid (s-ACSF) solution (206 mM sucrose, 2 mM KCl, 1 mM $MgCl_2$, 2 mM $MgSO_4$, 1.25 mM NaH_2PO_4, 26 mM $NaHCO_3$, 10 mM D-glucose, 1 mM $CaCl_2$). After 1-2 mins, the brain was glued onto a cutting stage such that the cortex faced the approaching blade. A piece of agarose gel was used as a cushion against the ventral part of the brain to prevent movement while cutting. Slices of 350 μm thick were cut with a Vibratome (Leica VT1200S; Leica, Nusslock, Germany) while the brain was submerged in a 4 ^{o}C cutting solution. The slices were then incubated at 32 ^{o}C for 1 hour in a gridded chamber filled with oxygenated incubating ACSF (124 mM NaCl, 3 mM KCl, 2 mM $MgSO_4$, 1.25 mM NaH_2PO_4, 26 mM $NaHCO_3$, 10 mM D-glucose, 1 mM $CaCl_2$). Each slice was kept in a grid of the chamber for up to 4 hours during an experiment.

Calcium imaging of spontaneous and glutamate uncaging-induced activities of cortical slices: A custom-built recording chamber was made by attaching a temperature control heated well (Thermal Well Temperature Controller TC-100, BioScience Tools, San Diego, CA) onto a cover slip. A liquid inflow tubing and a vacuum outflow tubing were installed to generate ACSF circulation through the chamber. A cortical slice was placed in the chamber and secured with a metal ring. Calcium activities of the slice was imaged with a system consisting of a Leica DM6000 FS upright microscope with a Leica EL-6000 120W mercury fluorescence light source directed through a 10x water submerge objective. Videos were capture with an iXON EMCCD DU-88U camera system (Andor USA, Concord, MA). Cortical layer 2/3 and layer 5 of the slices were imaged in one of the following

conditions: (1) high potassium ACSF (124 mM NaCl, 5 mM KCl, 2 mM $MgSO_4$, 1.25 mM NaH_2PO_4, 26 mM $NaHCO_3$, 10 mM D-glucose, 1 mM $CaCl_2$), (2) regular ACSF with 20 µM bicuculline, (3) regular ACSF with 20 µM bicuculline/ 20 µM DNQX, or (4) regular ACSF with 20 µM bicuculline/ 50 µM AP5.

To use glutamate uncaging to evoke neuronal activity in cortical slices, a frequency tripled Nd: YVO_4 UV laser (series 3500 pulse laser, ~1W, 100KHz repetition rate; DPSS Laser, San Jose, CA) was interfaced with a fiber optic submerged in the slice recording chamber and pointed directly at a cortical area on the slice. A solution of 100 µM of MNI-caged glutamate (4-methoxy-7-nitroindolinyl-caged L-glutamate; Toris Bioscience, Minneapolis, MN) in ACSF was used in each experiment. Focal photolysis of caged glutamate was accomplished by switching the UV laser to give a 400- to 800- µs light stimulus.

Analysis of calcium imaging data: Videos of calcium imaging were analyzed post hoc using NIH ImageJ software with a Time Series Analyzer plugin (Balaji J. UCLA). Only active cells that produced calcium fluorescence flashes at least once during an imaging period were analyzed. For each individual cell, the soma was manually circled, and three separate background regions were chosen by drawing circles of the same diameter in the surrounding area. The selected background areas did not include any dendrites or other neuronal structures. The true calcium fluorescence signal of a cell body or dendrites ΔF/F was calculated with an equation (1) excerpted from Chen et al.[18] that was developed by Kerlin et al.[19]:

$$\frac{\Delta F}{F} = \frac{(F_{true} - B)}{} \qquad \textbf{(Eq.1)}$$

where F_B is the baseline fluorescence averaged over three different regions surrounding the cell of interest and r is the contamination ratio standard constant 0.7. These data were then used to construct calcium transient profiles using OriginPro 9.1 (OriginLab, Northampton, MA). Peak amplitudes, frequencies, and durations were obtained with a Peak Analysis toolbox of OriginPro9.1. In short, responding peaks were picked first by setting minimum response threshold of 20% with respect to the highest amplitude peak of

that spectrum. The selected peaks were then compared with its corresponding video to confirm calcium activities. Peak analysis toolbox then calculated the amplitudes, frequencies, and durations at half maximum height for all events in the spectrum.

Statistics: Final plots were developed in Microsoft Excel and values are reported as mean ± S.E.M. All statistical analyses were done with Jmp Analysis 11 (SAS Institute Inc. 2013. Cary, NC) and GraphPad Prism 6 (GraphPad Software, La Jolla, California). ANOVA analyses were used for comparing numbers of total active spots of optogenetic mapping data (Repeated measures Anova), response amplitudes of motor maps (one-way), and amplitudes, frequencies and durations of calcium imaging data (one-way), and for comparing calcium amplitudes, frequencies, and durations among control, DNQX, and APV treated groups (two-way). For comparisons that yield statistical significances, Tukey's HSD post-hoc analyses were applied for further comparisons between specific groups. For glutamate uncaging data, a Pearson Chi-square's frequency test was used to compare percentages of active cells among groups at different time points after mTBI.

Results

mTBI resulted in reduced ipsilateral motor map at 2 hours but enhanced contralateral map at 12 hours post-mTBI

We employed a CCI device to generate a model of closed head mTBI in the mice. To assess motor functional changes after closed-head mTBI, we utilized optogenetic mapping to monitor potential changes in cortical motor map longitudinally. As a control, we mapped uninjured ChR2-expressing mice at various time points to assess the stability of this technique. In these mice, we found no significant change in the shape and size of the maps in 24 hours after initial mapping (Figure 1A), and the numbers of light responsive spots at 2h, 12h, and 24h did not change significantly (Figure 1B, $p > 0.05$, Repeated measures ANOVA, $n = 7$).

To determine longitudinal changes in cortical motor map after mTBI, recordings of optogenetically evoked EMG responses were made from the same ChR2-expressing mice at baseline, and 2h, 6h, 12h, and 1d, 3d, and 5d after injury. We found a significant

reduction in the numbers of light responsive spots at 2 h post-injury on the ipsilateral (i.e. ipsi-lesional) cortex (~50% reduction vs. baseline, $p < 0.01$, repeated measures ANOVA, Figure 2). In contrast, cortical map size on the contralateral cortex did not decrease at 2 h after injury but was significantly larger at 12h after injury (~20% increase vs. baseline, $p < 0.05$, repeated-measures ANOVA, Figure 2). The cortical maps of both hemispheres returned to baseline level at 72h and 120 h after mTBI (Figure 2).

We also assessed the changes in the average amplitudes of evoked EMG events by calculating mean amplitudes at each distance with respect to the anterior-to-posterior direction and medial-to-lateral direction (Figure 3). At 2 h post-mTBI, the average EMG amplitudes of ipsilateral forelimb was significantly lower than those of the baseline maps (Figure 3A, B). The lowest average response amplitudes (~0.2 ± 0.03 mV) were found to be around 1.5 mm lateral and 3.5 mm posterior to the bregma, which correlated to the region surrounding the injury epicenter (Figure 3A and B, $p < 0.05$, one-way ANOVA). However, we found that the average EMG amplitudes of contralateral forelimb at 12 h post-mTBI showed no significant difference compare to those of baseline responses (one-way ANOVA, Figure 3C and D).

Calcium imaging of GCaMP6 cortical slices revealed decreased ipsilateral calcium signals 2 h after mTBI

To determine whether the loss of ipsilateral motor map after mTBI was attributable to reduced cortical neuronal excitability, we employed calcium imaging to examine neuronal activity of cortical slices prepared in 2 h post-mTBI from ipsilateral hemisphere of GCaMP6 transgenic mice. Calcium imaging of cortical slices were done in an ACSF containing 5 mM potassium chloride to slightly promote neuronal activity for in vitro imaging. Comparing to the sham or contralateral cortex, neurons in cortical slices from injured brain usually showed single, slower and lower amplitude calcium transients (Figure 4A). They had significantly lower average amplitude of calcium responses than those of the sham animals (average $\Delta F/F$ amplitude 0.073 ± 0.015 vs. 0.120 ± 0.010 for 2h after mTBI group and sham group respectively, $p < 0.05$, one-way ANOVA, Figure 4A and B). There was no significant change in peak amplitude on the contralateral cortex (Figure 4A, and B). There was also a

large increase in the mean duration of calcium transients of neurons from slices of ipsilateral cortex but not contralateral (64.9 ± 17.7 ms, 98.3 ± 21.5 ms, and 175.8 ± 12.3 ms for sham, contralateral, ipsilateral slices respectively, $p<0.05$ for ipsilateral vs. sham groups, one-way ANOVA, Figure 4A and C), but there were dramatic decreases in the frequencies of calcium transients in both ipsilateral and contralateral cortices after mTBI, with the neurons of ipsilateral cortex having more decrease (~1±0.12 peak/cell ipsilateral vs. ~7±1.3 peak/cell contralateral vs. ~24 peak/cell sham at 2h, $p <0.05$, one-way ANOVA, Figure 4D). The undercurve area of the ipsilateral cortical neurons was significantly higher than that of the sham group (1.83±0.43 vs. 0.52±0.14 at 2h for ipsilateral vs. sham, $p <0.05$, one-way ANOVA, Figure 4E).

Reduction in AMPARs and NMDARs calcium signals in cortical slices at 2h post-mTBI

We further assessed the contribution of NMDARs and AMPARs to the lost activity of the injured cortex. Cortical slices from GCaMP6 mice were first imaged in the presence of 20 µM bicuculline to reveal spontaneous activities. There were significant decreases in the average amplitude and frequency of calcium transients, and an increase in calcium duration in the injured slices (Figure 5). Upon addition of 20 µM DNQX, there was a significant reduction in signal amplitude in both groups of the control and mTBI groups (0.062 ± 0.006 vs. 0.052 ± 0.009 for before and after DNQX of the control group, respectively and 0.04 ± 0.007 vs. 0.026 ± 0.004 for before and after DNQX of the mTBI group, respectively, $p<0.05$, two-way ANOVA; Figure 5A-B). However, the injured slices showed a much larger reduction comparing to the control group, ~50% reduction (0.026 ± 0.004 of mTBI DNQX vs 0.052 ± 0.009 of control DNQX, $p < 0.05$, two-way ANOVA). When 50 µM AP5 was added, an even larger reduction in calcium amplitude occurred in the injured slices, about 60% reduction (0.01 ± 0.004) comparing to the control slices (0.029 ± 0.003) ($p < 0.05$, two-way ANOVA, Figure 5A-B). The duration of calcium transients became significantly longer post-mTBI (~ 84.8 ± 6.29 ms vs ~ 71.2 ± 5.15 ms of control) and remained high even with addition of DNQX (42.8 ± 8.82 ms vs. 26.6 ± 3.33 ms of control. $p < 0.05$, two-way ANOVA, Figure 5C). Addition of AP5 produced no noticeable changes. Changes in response frequency of the injured group were similar to those of the response amplitude, with a significant reduction in injured slices (~3.28 ± 0.34 peaks/cells vs 6.23 ±

1.24 peaks/cells of control, p<0.05, two-way ANOVA) and further reductions after the addition of DNQX or AP5 (1.50 ± 0.69 peaks/cells and 1.06 ± 0.17 peaks/cells of injury group, respectively vs. ~2.84 ± 0.44 peaks/cells and 1.89 ± 0.25 of control group, respectively, p < 0.05, two-way ANOVA); (Figure 5D).

Glutamate uncaging of GCaMP6 cortical slices revealed reduced calcium signals and impaired AMPARs and NMDARs function

To directly assess the function of glutamate receptors, we employed glutamate uncaging technique to activate glutamate receptors in cortical slices at multiple time points (Figure 6). Calcium transients of the injured slices at all time points had significant decreases in amplitude compared to sham slices at 2h after mTBI (0.034 ± 0.002 vs 0.087 ± 0.01 of sham, p <0.05, one-way ANOVA), 12h after mTBI (0.030 ± 0.001 vs. 0.087 ± 0.01 of sham), and worsen at 24h (0.026 ± 0.003 vs. 0.087 ± 0.01 of sham p <0.05, one-way ANOVA) after mTBI (Figure 6B). The duration of calcium transient was significantly longer for at all time points (244.5 ± 26.9 ms of 2h, 490.1 ± 89.9 ms of 12h, and 460.7 ± 78.4 ms of 24h vs. 99.7 ± 5.93 ms of sham, p < 0.05, one-way ANOVA, Figure 6C). Furthermore, we noticed gradual increases in the latency period from glutamate uncaging to calcium responses over time after mTBI. In sham slices, 88.3 % of the responsive neurons had latency periods of less than 200 ms. After mTBI, only ~69%, 37 %, and 28.6 % of the responsive neurons from the 2h, 12h, and 24h groups, respectively, had latency periods of less than 200 ms (p<0.001 for control vs. 2h, 12h, and 24h and p<0.05 for 2h vs. 12h and 24h, Pearson Chi-square test, Figure 6D). Consistently, increasingly higher percentages of neurons in later mTBI groups had latency periods between 200-500 ms (11.8 %, 30.4%, 42.6%, and 64.3% for sham, 2h, 12h, and 24h groups after mTBI, respectively, p<0.001 for sham vs. 2h, 12h, and 24h, p<0.05 for 2h vs. 24h and 12h vs. 24h , Pearson Chi-square test Figure 6E).

Discussion

Individuals who suffer from mTBI exhibit short-term functional deficits in the absence of significant neuronal death and have been observed to recover in chronic stage[20-22]. The traumatized but surviving neurons may play a role in the functional deficits and recovery of the injured brain. In this study, we have demonstrated that closed-head mTBI in mice

caused a transient activity loss of cortical motor map in vivo, which is attributable to depressed cortical neuronal activity due to impaired NMDA and AMPA receptor functions and calcium homeostasis.

This study is the first study to use repeated in vivo optogenetic motor mapping technique as a functional readout to evaluate longitudinal changes in motor function after mTBI. This highly efficient technique provides a reproducible and minimally invasive approach for generating functional maps to obtain insights into the electrophysiological properties and longitudinal changes of the corticospinal pathway[4-6]. Using this novel approach, we found mTBI resulted in a significant loss in cortical motor map in 2 hours after trauma. This result is consistent with previous behavioral findings in animals showing loss of righting reflex up to at least 2 hours after injury[23] and impaired motor function during rotarod test for up to one day[24]. Our results also support previous findings in concussion patients who was shown to suffer increased cortical silence period, indicative of long term intra-cortical inhibition[25] and in football athletes who sustained concussions performed significantly worse in dexterity, reaction, and movement tests[26]. Interestingly, the motor map of the uninjured contralateral hemisphere had a significant increase in map size in 12 h post-mTBI. This suggests there may be a compensatory mechanism in response to the hypo-activity of the injured cortex.

Our in vivo longitudinal mapping results confirm that closed-head mTBI induces hypoexcitability of the injured cortex. In contrast, there have been many reports of hyperexcitability in the acute phase of TBI due to increased release of glutamate and excitotoxicity that may cause subsequence loss of cortical function[27, 28]. However, the increase in extracellular glutamate is transient, lasting from only a few minutes in mild TBI[10] to half an hour in more severe TBI[9]. Several clinical trials, such as the Selfotel trials in particular, were undertaken to block neuronal hyperexcitability with different glutamate receptor antagonists, but the results were inconsistent, with some of them even showing detrimental effects[14, 15, 29]. In contrast, several studies found that the expression of ionotropic glutamate receptors, including NMDA receptors[11, 30] and AMPARs[13], actually decrease after brain injury. The loss of these receptor expressions peaks during the first 24 hours post-injury and lasts for 7 days[12, 31, 32]. Furthermore, these losses could be attributed

to reduction in surface expression of NMDA receptors subunits NR1/NR2A/NR2B[33], AMPA receptor subunit GluR1[34], and down-regulations of receptor synthesis[32]. Consistently, activating AMPA or NMDA receptors during the acute phase after injury improves functional outcomes of animals with a wide range of TBI severities[11, 35].

Since calcium is a major intracellular signaling molecule in neurons, alterations in calcium homeostasis could have significant effects on neuronal physiology and network activity. Therefore, the assessment of glutamate receptors function, a major contributor to neuronal calcium transient, is an important step in understanding how brain activity changes following trauma. Using in vitro imaging of cortical slices from GCamP6 transgenic mice, we showed a loss in spontaneous cortical neuronal calcium signals shortly after injury and this loss occurred mainly in the injured hemisphere but not in the contralateral hemisphere in 2 hours after injury. This is consistent with recent evidence of reduced calcium dynamics during the acute phase in a blast brain injury model[36]. An increase in the duration of calcium transients in the injured cortex points to a longer retention of Ca^{2+} in the cytosol. This change in intracellular Ca^{2+} clearance may be a compensatory mechanism, or more likely, an impairment in calcium regulation between cytosol and the extracellular space or with intracellular calcium storage (i.e. endoplasmic reticulum (ER) and mitochondria). Earlier studies in hippocampal CA3 neurons after a fluid percussion TBI have shown that prolonged retention of Ca^{2+} in the cytosol could be due to impaired calcium clearance[22, 37]. This cytosolic calcium dysregulation after TBI could be attributed to impairments in calcium buffering capacity, neuronal membrane Na/Ca exchanger, and intracellular ER/mitochondria storage[38, 39]. For example, mechanically induced injury has been shown to alter mitochondrial membrane potential and reduce ATP levels in neurons in the absence of hypoxia[40, 41]. A reduction in ATP severely affects the role of sarco/endoplasmic reticulum calcium ATPase (SERCA) and plasma membrane calcium ATPase (PMCA) in pumping Ca^{2+} either into storage (ER/mitochondria) or into extracellular space and results in Ca^{2+} accumulations for longer time in cytosol[40, 42]. When blocking NMDA receptors with AP5 to assess AMPAR-dominant calcium transient, we found almost 60% reduction in calcium transient compare to about 50% by DNQX. This indicates the majority of calcium influx from the extracellular space occurs through NMDAR receptors

and NMDARs impairment may be responsible for majority of the signal decline in mTBI-induced loss of calcium signals. Our results are consistent with an earlier report of a 20-40% loss in NMDA receptor expressions in cortex hippocampus in 5 minutes to up to 24 hours after fluid percussion induced-TBI[12]. Furthermore, they also found AMPA receptor expression level reduced at similar level (~25% loss from baseline) from 5 minutes up to 3 hours after trauma but recover to normal level in 24 hours. Future investigation using whole-cell patch clamp recordings may provide more precise measurements of changes in AMPA and NMDA receptor function after mTBI.

The use of glutamate uncaging technique allowed us to directly test changes in the function of major glutamatergic calcium channels of NMDAR and AMPAR after mTBI. These glutamate-derived calcium influxes reduced at 2h and remained low at later time up to 24 hours after trauma. In addition, calcium signals in response to glutamate uncaging was dramatically altered, with faster responses being increasingly replaced by slower ones at later time points post-mTBI. This further suggests that impairment of glutamatergic ion channels such as NMDAR and AMPAR persist long after mTBI. This longer lasting impairment of NMDAR could contribute to long-term synaptic dysfunction. Since the impairment in NMDA receptors lasted for a longer time period, the functional recovery of the in vivo motor maps could be attributed to reduction of cortical inhibition[43] and recovery of other glutamate receptors such as AMPARs[44], which may increase the influx of Na^+ into cells to cause membrane depolarization[45].

Although functional changes after mTBI are often transient and followed by functional recovery at a later time point, understanding these early changes after a single mild injury may help us to understand changes after repeated and more severe injuries. Similar to the spontaneous calcium signals, the duration of calcium signals evoked by glutamate uncaging became longer for all time points after mTBI. While current data do not answer which factors contribute to changes in cytosolic calcium signal, intracellular calcium channels such as ryanodine receptors (RyR), SERCA pumps of ER, and calcium uniporters of mitochondria may play a potential role in regulating intracellular calcium post-mTBI[42, 46, 47]. Interestingly, prolonged elevations and retention of intracellular calcium, while not leading

to neuronal death, have been demonstrated to cause alterations in neuronal excitability[48, 49] and long-term changes in gene expression[50, 51] even during the acute phases of TBI[52-54].

As the most common form of brain trauma, mTBI can produce acute and transient effects, which may subsequently contribute to long lasting sequelae, especially in cases where multiple mTBI occurs over a short period of time. Using a combination of in vivo optogenetic motor mapping, activity imaging in cortical slices from GCaMP6 transgenic mice, and glutamate uncaging, this study demonstrates transient deficit in the function of motor cortex in vivo after mTBI and the contribution of impaired glutamate receptor function. With our novel approach to mTBI using optogenetic mapping, our study shows that mTBI induced short-term neuronal ***hypo***excitability in injured cortex, as indicated by the loss of motor maps and the smaller and longer-lasting calcium transients. We also found that the impairments in calcium signals are attributable to a reduction in the activities of NMDA receptors and AMPA receptors and impaired intracellular calcium homeostasis. A deeper understanding of the mechanisms that alter neuronal calcium homeostasis in the injured brain may offer novel therapeutic strategies to effectively relieve morbidities associated with mTBI.

Acknowledgements

We thank Dr. Xingjie Ping for her assistance and technical expertise. This work was supported by grants from NIH NS057940 & NS089509 and by the Indiana Spinal Cord and Brain Injury Research Fund.

Author Disclosure Statement

The authors declare that the research was conducted in the absence of any commercial or financial relationships that could be construed as a potential conflict of interest.

References:

1. Roozenbeek, B., Maas, A. I., Menon, D. K. (2013). Changing patterns in the epidemiology of traumatic brain injury. Nature Reviews Neurology 9, 231-236.

2. Povlishock J.T., K.D.T. (2005). Update of neuropathology and neurological recovery after traumatic brain injury. Journal of Head trauma rehabilitation 20, 76-94.

3. Graham D.T., M.T.K., Maxwell W.L., Nicoll, J.A. (2000). Recent advances in neurotrauma. Journal fo Neuropathological Epxerimental Neurology 59, 641-651.

4. Oliver G S Ayling, T.C.H., Jamie D Boyd, Alexander Goroshkov, Timothy H Murphy (2009). Automated light-based mapping of motor cortex by photoactivation of channelrhodopsin-2 transgenic mice. Nature Methods 6.

5. Qian J., W.W., Xiong W., Chai Z., Xu XM., Jin X. (2019). Longitudinal Optogenetic Motor Mapping Revealed Structural and Functional Impairments and Enhanced Corticorubral Projection after Contusive Spinal Cord Injury in Mice. Journal of Neurotrauma 36, 485-499.

6. Omlor W., W.A.S., Sipila P., Lutcke H., Laurenczy B., Chen IW., Sumanovski LT. van't-Hoff M., Bethge P., Voigt FF., Schwab ME., Helmchen F. (2019). Context-dependent limb movement encoding in neuronal populations of motor cortex. Nature Communications 10, 4812.

7. Arundine M., T.M. (2004). Molecular mechanisms of glutamate-dependent neurodegeneration in ischemia and traumatic brain injury. Cell Molecular Life Science 61, 657-668.

8. Yi J.H., H.A.S. (2006). Excitotoxic mechanisms and the role of astrocytic glutamate transporters in traumatic brain injury. Neurochemistry International 48, 394-403.

9. ALAN I. FADEN, P.D., S. ScoTT PANTER, ROBERT VINK (1989). The Role of Excitatory Amino Acids and NMDA Receptors inTraumatic Brain Injury. Science 244, 394-403.

10. Pelle Nilsson, E.R.-E., Roland Flink, Urban Ungerstedt, Hans Carlson, Lars Hillered (1994). Epileptic seizure activity in the acute phase following cortical impact trauma in rat (Glutamate level post TBI). Brain Research 637, 227-232.

11. Biegon A., P.A.F., Charles M. Paden, Alexander Alexandrovich, Jeanna Tsenter, Esther Shohami (2004). Dynamic changes in N-methyl-D-aspartate receptors after closed head injury in mice: Implications for treatment of neurological and cognitive deficits. PNAS 101, 5117-5122.

12. L.P. Miller, B.G.L., L.W. Jenkins , L. Oleniak, D. Panchision, R.J. Hamm, L.L. Phillips, C.E. Dixon, G.L. Clifton, R.L. Hayes (1990). Excitatory amino acid receptor subtype binding following traumatic brain injurys. Brain Research 526, 103-107.

13. Paulette B. Goforth, J.R., Benjamin S. Schwartz, Leslie S. Satin (2011). Excitatory synaptic transmission and network activity are depressed following mechanical injury in cortical neurons. Journal of Neurophysiology 105, 2350-2363.

14. Chrysanthy Ikonomidou, L.T. (2002). Why did NMDA receptor antagonists fail clinical trials for stroke and traumatic brain injury? The Lancet Neurology 1.

15. G. Morris, R.B., S. Marshal, A. Marmarou, A. Maas, L. Marshall (1999). Failure of competitive N-methyl-D-aspartate antagonist Selfotel (CGS 19755) in the treatment of severe head injury: results of two Phase III clinical trials. Journal of Neurosurgery 91, 737-743.

16. Jennifer A. Creed, A.M.D., Douglas P. Fox, Alan R. Tessler, Ramesh Raghupathi (2011). Concussive Brain Trauma in the Mouse Results in Acute Cognitive Deficits and Sustained Impairment of Axonal Function. Journal of Neurotrauma 28, 547-563.

17. Han X., C.Z., Ping X., Song L., Ma C., Ruan Y., Jin X. (2020). In vivo two-photon imaging reveals acute cerebral vascular spasm and microthrombosis after mild traumatic brain injury in mice. frontiers in Neuroscience.

18. Tsai-Wen Chen, T.J.W., Yi Sun, Stefan R. Pulver, Sabine L. Renninger, Amy Baohan, Eric R. Schreiter, Rex A. Kerr, Michael B. Orger, Vivek Jayaraman, Loren L. Looger, Karel Svoboda, Douglas S. Kim (2013). Ultrasensitive fluorescent proteins for imaging neuronal activity. Nature 499.

19. A. Kerlin, M.A., V. Berezovskii, R.C. Reid (2010). Broadly tuned response properties of diverse inhibitory neuron subtypes in mouse visual cortex. Neuron 67, 858-871.

20. Delahunty TM. , J.J., Gong QZ. , Black RT. , Lyeth BG. (1995). Differential consequences of lateral and central fluid percussion brain injury on receptor coupling in rat hippocampus. Journal of Neurotrauma 12, 1045-1057.

21. Zohar, O., Rubovitch, V., Milman, A., Schreiber, S. and Pick, C.G. (2011). Behavioral consequences of minimal traumatic brain injury in mice. Acta Neurobiol Exp (Wars) 71, 36-45.

22. David A. Sun, L.S.D., Sompong Sombati, Anya Baranova, Margaret S. Wilson, Robert J. Hamm, and Robert J. DeLorenzo (2008). Traumatic brain injury causes a long-lasting calcium Ca plateau of elevated intracellular Ca levels and altered Ca homeostatic mechanisms in hippocampal neurons surviving traumatic brain injury. European Journal of Neuroscience 27, 1659-1672.

23. Antal, J., d'Amore, A., Nerozzi, D., Palazzesi, S., Pezzini, G. and Loizzo, A. (1992). An EEG analysis of drug effects after mild head injury in mice. Life Sci 51, 185-193.

24. Yung Chia Chen, H.M., King H. Yang,Ted Abel, David F. Meaney (2014). A modified controlled cortical impact technique to model mild traumatic brain injury mechanics in mice. Frontiers in Neurology 5.

25. Nick R. Miller, A.L.Y., Logan F. Maynard, Li-Shan Chou, David R. Howell, Anita D. Christie (2014). Acute and longitudinal changes in motor cortex function following mild traumatic brain injury. Brain Injury 28, 1270-1276.

26. Alan J. Pearce, K.H., Mark A. Rogers, Daniel T. Corp, Jerome J. Maller, Hannah G.K. Drury, Paul B. Fitzgerald (2014). The Long-Term Effects of Sports Concussion on Retired Australian Football Players: A Study Using Transcranial Magnetic Stimulation. Journal of Neurotrauma 31, 1139-1145.

27. C. Edward Dixon, W.C.T., Ronald L. Hayes (1993). Mechanisms of mild traumatic brain injury. Journal of Head trauma rehabilitation.

28. Jennifer M. Spaethling, D.M.K., Pallab Singh, David F. Meaney (2008). Calcium-Permeable AMPA Receptors Appear in Cortical Neurons after Traumatic Mechanical Injury and Contribute to Neuronal Fate. Journal of Neurotrauma 25, 1207-1216.

29. Farin A., M.L. (2004). Lessons from epidemiologic studies in clinical trials of traumatic brain injury. Acta Neurochirurgica Supplement 89, 101-107.

30. Grossman, R., Shohami, E., Alexandrovich, A., Yatsiv, I., Kloog, Y. and Biegon, A. (2003). Increase in peripheral benzodiazepine receptors and loss of glutamate NMDA receptors in a mouse model of closed head injury: a quantitative autoradiographic study. Neuroimage 20, 1971-1981.

31. Sihver, S., Marklund, N., Hillered, L., Langstrom, B., Watanabe, Y. and Bergstrom, M. (2001). Changes in mACh, NMDA and GABA(A) receptor binding after lateral fluid-percussion injury: in vitro autoradiography of rat brain frozen sections. J Neurochem 78, 417-423.

32. Friedman, L.K., Ginsberg, M.D., Belayv, L., Busto, R., Alonso, O.F., Lin, B., Globus, M.Y. (2001). Intra-ischemic but not postischemic hypothermia prevents non-selective hippocampal downregulation of AMPA and NMDA receptor gene expression after global ischemia. Brain Research 86, 34-47.

33. Arvind Kumar, L.Z., Xiaoqing Yuan, Yan Long, Keyi Yang (2002). N-Methyl-D-Aspartate Receptors: Transient Loss of NR1/NR2A/NR2B Subunits After Traumatic Brain Injury in a Rodent Model. Journal of Neuroscience Research 67, 781-786.

34. Johanna Schumann, G.A.A., Anat Biegon, and Rami Yaka (2008). Inhibition of NR2B Phosphorylation Restores Alterations in NMDA Receptor Expression and Improves Functional Recovery following Traumatic Brain Injury in Mice. Journal of Neurotrauma 25, 945-957.

35. Chrysanthy Ikonomidou, V.S., Lechoslaw Turski (2000). Neuronal death enhanced by N-methyl-D- aspartate antagonists. PNAS 97, 12885-12890.

36. Hansen K., D.G., Mohammed A., Tseng H., Abdulkerim M., Bensussen S., Saligrama V., Nazer B., Eldred W., Han X. (2018). Mild blast injury produces acute changes in basal intracellular calcium levels and activity patterns in mouse hippocampal neurons. Journal of Neurotrauma 35, 1523-1536.

37. Slemmer J.E., S.J.J., Sweeney M.I., Weber J.T. (2008). Antioxidants and free radical scavengers for the treatment of stroke, traumatic brain injury and aging. Current Medicinal Chemistry 15, 404-414.

38. M. Brittain, T.B., N. Brutovesky (2013). Delayed calcium dysregulation in neurons requires both the NMDA receptor and the reverse Na/Ca exchanger. Neurobiology of Disease 46, 109-117.

39. J. Weber, B.R., E. Ellis (2000). Traumatic injury of cortical neurons causes changes in intracellular calcium stores and capacitative calcium influx. Journal of Biological Chemistry 276, 1800-1807.

40. Tavalin S.J., E.E.F., Satin L.S. (1997). Inhibition of the electrogenic Na pump underlies delayed depolarization of cortical neurons after mechanical injury or glutamate. Journal of Neurophysiology 77, 632-638.

41. Ahmed S.M., W.J.T., Liang S., Willoughby K.A., Sitterding H.A., Rzigalinski B.A., Ellis E.F. (2002). NMDA receptor activation contributes to a portion of the decreased mitochondrial membrane potential and elevated intracellular free calcium in strain-injured neurons. Journal of Neurotrauma 19, 1619-1629.

42. Parsons J.T., C.S.B., DeLorenzo R.J. (1997). Ischemia-induced inhibition of calcium uptake into rat brain microsomes mediated by Mg2+ /Ca2+ ATPase. Journal of Neurochemistry 68, 1124-1134.

43. Hsieh TH, L.H., Hameed MQ, et al. (2017). Trajectory of parvalbumin cell impairment and loss of cortical inhibition in traumatic brain injury. Cereb Cortex 27, 5509-5524.

44. Goforth P.D., E.F.F., Satin L.S. (2004). Mechanical injury modulates AMPA receptor kinetics via an NMDA receptor-dependent pathway. Journal of Neurotrauma 21, 719-732.

45. Wolf J.A., S.P.K., Lusardi T., Meaney D., Smith D.H. (2001). Traumatic axonal injury induces calcium influx modulated by tetrodotoxin-sensitive sodium channels. Journal of Neuroscience 21, 1923-1930.

46. J., W. (2012). Altered calcium signaling following traumatic brain injury. Frontiers in Pharmacology 3, 60.

47. David D. Limbrick Jr. , S.P., Robert J. DeLorenzo (2001). Hippocampal neurons exhibit both persisten Ca influx and impairment of Ca sequestration/extrusion mechanisms following 21 excitotoxic glutamate exposure. Brain Research 894, 56-67.

48. D.A Sun, S.S., R.E. Blair, R.J. Delorenzo (2002). Calcium dependent epileptogeneiss in an in vitro model of stroke-induced epilepsy. Epilepsia 43, 1296-1305.

49. R.J. Delorenzo, D.A.S., L.S. Deshpande (2005). Cellular mechanisms underlying acquired epilepsy: the calcium hypothesis of the induction and maintenance of epilepsy. Pharmacological Ther. 105, 229-266.

50. T.A. Morris, N.J., A.C. Rice, O. Vasconcelos, R.J. DeLorenzo (1999). Persistent increased DNA-binding and expression of serum response facgtor occur with epilepsy-associated long-term plasticity changes. Journal of Neuroscience 19, 8234-8243.

51. T.A. Morris, N.J., R.J. DeLorenzo (2000). Chronic deltaFos B expression and increased Ap-1 transcription factor binding are associated with long term plasticity changes in epilepsy. Brain Res. Mol. Brain Res. 79, 138-149.

52. R.L. Hayes, K.Y., R. Raghupathi, T.K. McIntosh (1995). Changes in gene expression following traumatic brain injury in rat. Journal of Neurotrauma 12, 779-790.

53. R. Raghupathi, T.K.M. (1996). Regionally and temporally distinct patterns of induction of c-fos, c-jun and junB mRNAs following experimental brain injury in rat. Brain Res 37, 134-144.

54. B. Morrison, J.H.E., D.F. Meaney, T.K. McIntosh (2000). Traumatic injury induces differential expression of cell death genes in organotypic brain slice cultures determined by complementary DNA array hybridization. Neuroscience 96, 131-139.

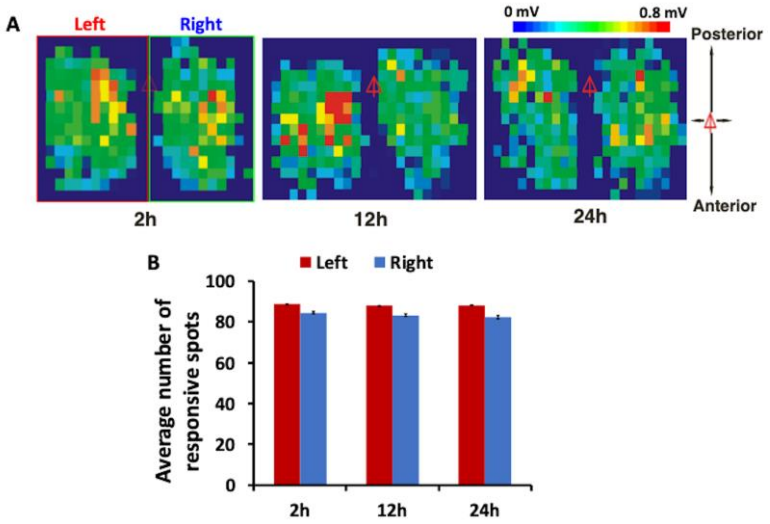

Figure 1: Repeated optogenetic mapping of motor cortex in a ChR2 mouse produced stable baseline motor maps in 24 hours. (A) Representative cortical motor maps of both left and right hemispheres from a sham mouse mapped at 2 hours, 12 hours, and 1 day after skull preparation. The red triangles indicate the position of bregma, and the color bar indicates different peak amplitudes of EMG response. While there existed variabilities in the shape and pattern of motor maps constructed based on EMP peak amplitudes, there were no significant changes in general map size over time. (B) There were no significant differences in average numbers of responsive spots in both cortical hemispheres at 2h, 12h, and 24h mapping times (n=7, mean ± S.E.M, repeated-measures ANOVA).

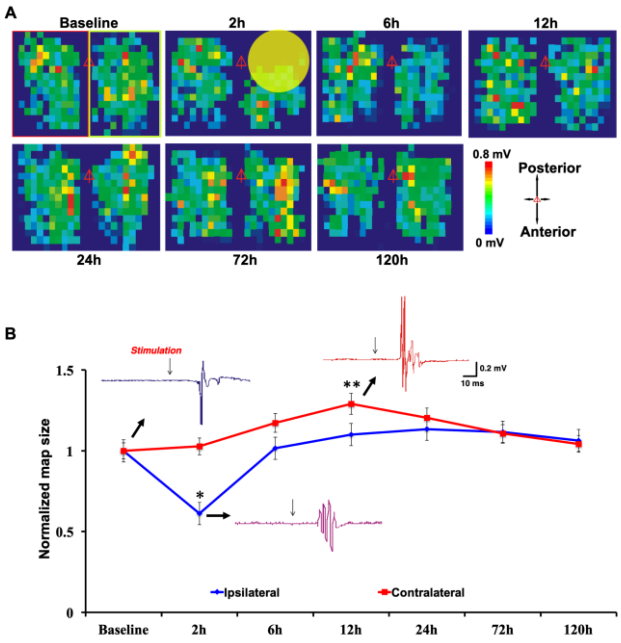

Figure 2: Optogenetic mapping revealed acute loss of motor map after mTBI followed by recovery of the ipsilateral cortex and transient hyperexcitability of the contralateral cortex. (A) Representative motor maps at baseline and different time points after closed-head mTBI. Note the loss of motor map at 2 hours after mTBI. The red triangles indicate position of bregma and color bars indicate strength of EMG response. The yellow circle indicates area of impact (approximately ~3mm). The green box (right side of map) indicates ipsilateral and red-box (left side of map) indicates contralateral. (B) Mean normalized map size showed that mTBI resulted in a decrease in motor map size (i.e. number of responsive spot) of the ipsilateral cortex at 2h after injury and recovery at 12h. In contralateral cortex, mTBI resulted in a transient increase in map size at 12 h post injury. Also shown are sample mapping traces of control and post-mTBI EMG responses. (*p<0.01, **p<0.05, mean ± S.E.M , Repeated measures ANOVA, Turkey's HSD post hoc, n = 7).

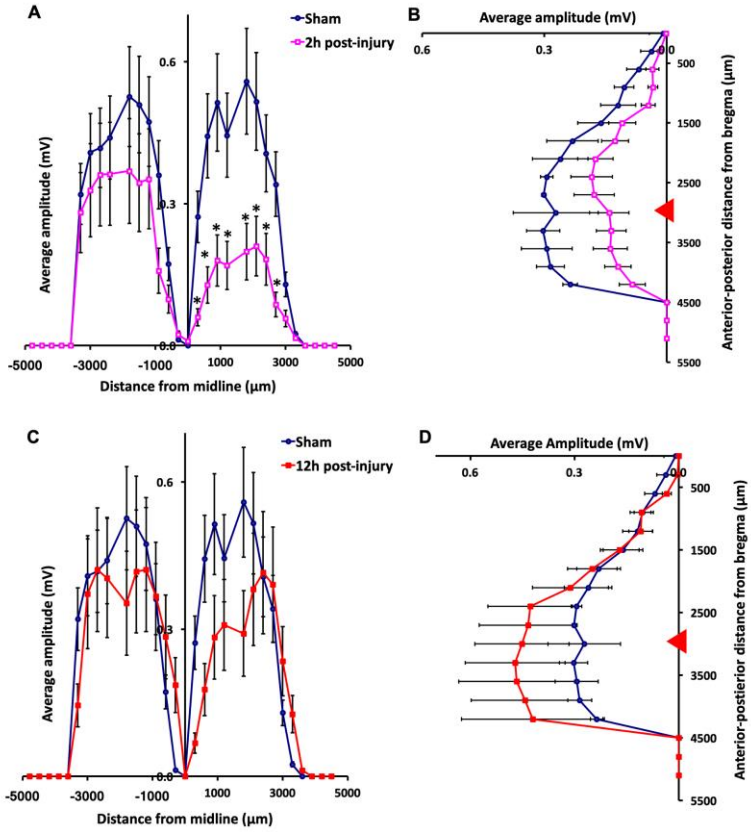

Figure 3: Decreased ipsilateral response intensity of motor map at 2h after mTBI. Plots present changes in motor responses along medial-lateral direction (A and B) and anterior-posterior direction (C and D). A-B. Decreases in light-evoke EMG amplitudes of ipsilateral cortex at 2h after mTBI (*$p<0.05$, mean ± S.E.M, one-way ANOVA, Tukey's HSD, n = 7). C-D. No significant differences in light-evoke EMG amplitudes of contralateral cortex at 12h after mTBI (n=7, mean ± S.E.M, one-way ANOVA). Horizontal axis in (A and C) presents medial-lateral positions and vertical axis in (B and D) presents posterior-anterior positions. The red-triangle in (B) and (D) represent position of bregma.

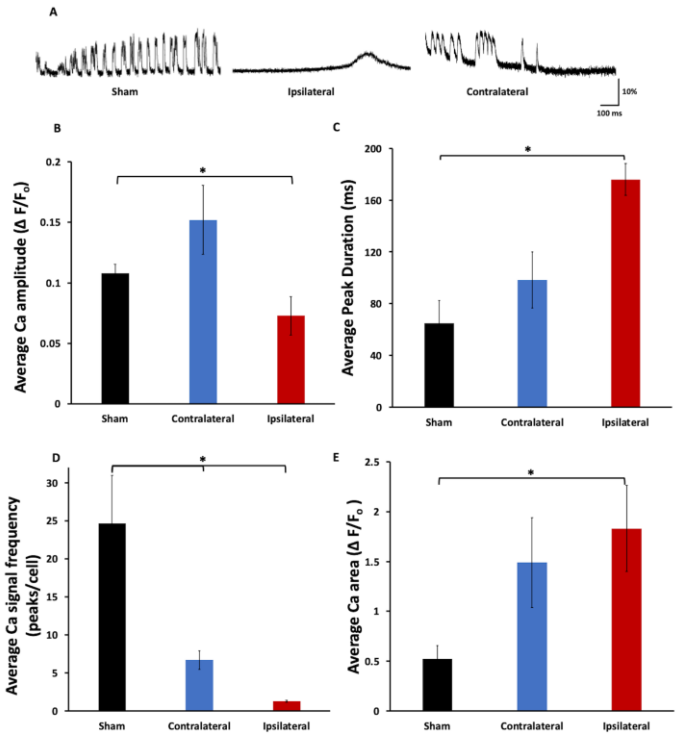

Figure 4: *Ex vivo* imaging of GCaMP6 cortical slices showed impairments of spontaneous calcium signals on the ipsilateral cortex 2h after mTBI. (A) Examples of spontaneous calcium traces cortical neurons at baseline and after injury. (B) There was a significant reduction in spontaneous calcium peak amplitude of neurons of ipsilateral cortex but no significant change in contralateral cortex at 2h after mTBI. (C) There was a significant increase in spontaneous calcium peak duration of neurons of ipsilateral cortex at 2h after mTBI. (n = 9 slices/group *p<0.05, mean ± S.E.M, one-way ANOVA, Turkey's HSD post hoc). (D) There were significant decreases in the frequencies of spontaneous calcium events of neurons of ipsilateral and contralateral cortices at 2h after mTBI (n = 9 slices/group *p<0.05, mean ± S.E.M, one-way ANOVA, Turkey's HSD post hoc). (E) There was a significant increase in the undercurve area of calcium events of ipsilateral cortical neurons at 2h after mTBI compare to sham (n = 9 slices/group *p<0.05, mean ± S.E.M, one-way ANOVA, Turkey's HSD post hoc)

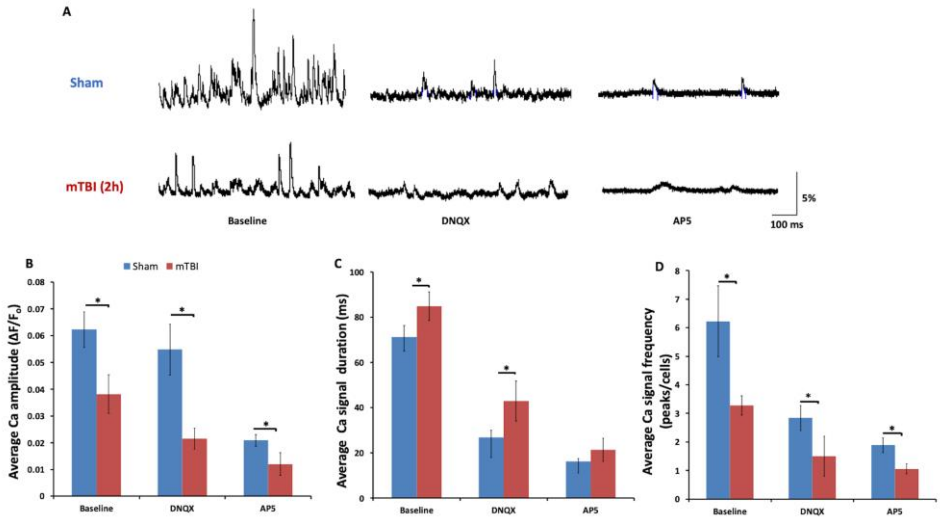

Figure 5: Calcium imaging of GCaMP6 cortical slices showed different losses of AMPA and NMDA receptor signals at 2h after mTBI. (A) Sample traces of spontaneous calcium transients of layer 5 cortical neurons after bicuculline, bicuculline+DNQX, and bicuculline+AP5 treatments. (B). There was a significant decrease in calcium peak amplitude at 2h after mTBI, with larger decreases after application of 50 µM AP5 in both sham and mTBI slices. (C). There were increases in calcium signal duration at 2h mTBI after mTBI and after application of 20 µM DNQX in the mTBI slices. (D) There were significant decreases in calcium signal frequencies at 2h after mTBI, and after application of DNQX or AP5. Scale bar: 400 µm, (*$p < 0.05$, mean ± S.E.M, two-way ANOVA, Turkey's HSD post hoc, n = 8 slices /group).

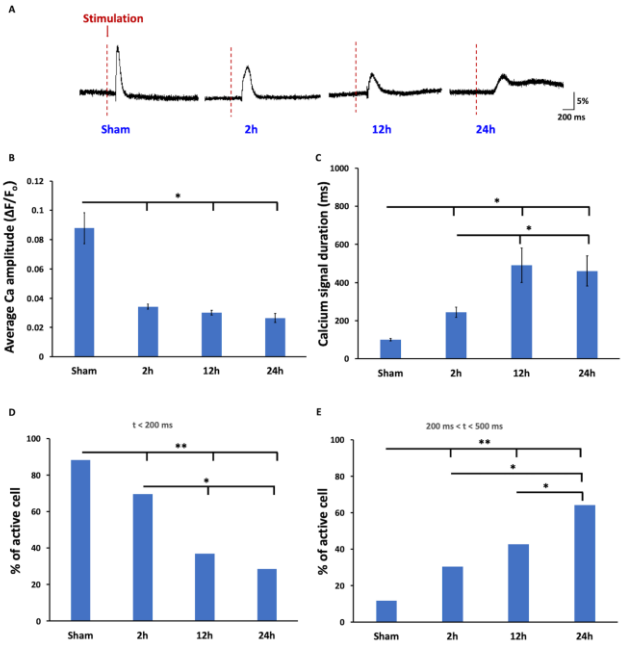

Figure 6: Glutamate uncaging in GCaMP6 cortical slices revealed reduced calcium signals with longer latency at 2h after mTBI. (A) Sample traces of calcium responses in slices evoked by glutamate uncaging at baseline, 2h, 12h, and 24h after mTBI. (B) mTBI resulted in significantly decreased calcium signal amplitudes at 2h, 12h, and 24h after injury. (C) mTBI resulted in significantly increased calcium signal duration at 2h, 12h, and 24h after injury. (* $p<0.05$, mean ± S.E.M, one-way ANOVA, Tukey's HSD, n = 11 slices/group). (D) The percentages of neurons with response latency < 200 ms became increasingly decreased at 2h, 12h, and 24h after injury. (E). The percentages of neurons with response latency between 200-500 ms became increasingly larger at 2h, 12h, and 24h after mTBI. (**$p<0.001$, *$p<0.05$, mean ± S.E.M, Pearsons Chi-square test)